Intercomparison of interannual changes in NDVI from PAL and GIMMS in relation to evapotranspiration over northern Asia

Rikie Suzuki, Kooiti Masuda, and Dennis Dye
Frontier Research Center for Global Change
3173-25 Showamachi, Kanazawa-ku Yokohama, Kanagawa 236-0001, Japan
rikie@jamstec.go.jp (R. Suzuki), masuda@jamstec.go.jp (K. Masuda), dye@jamstec.go.jp (D. Dye)

Abstract: The authors' previous study found an interannual covariability between actual evapotranspiration (ET) and the Normalized Difference Vegetation Index (NDVI) over northern Asia. This result suggested that vegetation controls interannual variation in ET. In this prior study, NDVI data from the Pathfinder AVHRR Land (PAL) dataset were analyzed. However, studies of NDVI interannual change are subject to uncertainty, because NDVI data often contain errors associated with sensor- and atmosphere-related effects. This study is aimed toward reducing this uncertainty by employing NDVI dataset, from the Global Inventory Monitoring and Modeling Studies (GIMMS) group, in addition to PAL. The analysis was carried out for the northern Asia region from 1982 to 2000.

19-year interannual change in PAL-NDVI and GIMMS-NDVI were both compared with interannual change in model-assimilated ET. Although the correlation coefficient between GIMMS-NDVI and ET is slightly less than for PAL-NDVI and ET, for both NDVI datasets the annual maximum correlation with ET occurs in June, which is near the central period of the growing season. A significant positive correlation between GIMMS-NDVI and ET was observed over most of the vegetated land area in June as well as PAL-NDVI and ET. These results reinforce the authors' prior research that indicates the control of interannual change in ET is dominated by interannual change in vegetation activity.
Keywords: Siberia, Taiga, climate system, phenology

1. Introduction

Vegetation over an extensive area influences actual evapotranspiration (ET) from the land to the atmosphere mainly through transpiration activity. The authors' previous study [8] found an interannual covariability between ET and the Normalized Difference Vegetation Index (NDVI), a remotely-sensed measure of vegetation greenness, over a continental-scale land surface. This result suggested that vegetation controls interannual variation in ET, and therefore vegetation change must be considered to predict future climate. In this prior study, NDVI data from the Pathfinder AVHRR Land (PAL) dataset were analyzed. However, studies of NDVI interannual change are subject to uncertainty, because NDVI data often contain errors associated with sensor- and atmosphere-related effects. This study is aimed toward reducing this uncertainty by employing a second major NDVI dataset, from the Global Inventory Monitoring and Modeling Studies (GIMMS) group, in addition to PAL. GIMMS-NDVI data were produced with a calibration method that differs from the one employed for PAL-NDVI data. An intercomparison of the PAL-NDVI and GIMMS-NDVI datasets provide an effective basis for further analysis of the covariability of NDVI and ET interannual changes.

2. Data and Method

The NDVI is defined as NDVI = $(Ch2 - Ch1)/(Ch2 + Ch1)$, where $Ch1$ and $Ch2$ are measurements from Advanced Very High Resolution Radiometer (AVHRR) channels 1 (visible) and 2 (near-infrared) of NOAA satellite, respectively. Analyses were conducted on the monthly basis from 1982 to 2000 over northern Asia (30°E – 150°E, 30°N – 75°N).

1) PAL NDVI

The NDVI value from 10-daily PAL dataset (1 × 1-degree spatial resolution) was examined. The monthly value was composited by choosing the highest NDVI among three 10-day datasets for each month. This process effectively removed cloud-contaminated observations. The 1 × 1-degree value was resampled into 2.5 × 2.5-degree grid system to link with the ET grid system.

The PAL data are adjusted for errors due to non-vegetative factors such as satellite orbit drift, sensor degradation, and ozone concentration and represent interannual variation in vegetation well. Atmospheric Rayleigh scattering and ozone absorption were corrected. Scan angle criteria is within +/– 42 degrees of nadir. The influence due to sensor degradation and orbital drift were adjusted according to the

empirical formula [6, 7]. Intercalibration with NOAA-9 and other NOAA was also conducted.

2) GIMMS NDVI

The NDVI value from 15-daily GIMMS dataset (8 × 8 km spatial resolution) [4, 5, 9] were examined to be compared with PAL-NDVI. First, the original 8km pixel value was resampled into 1 × 1-degree grid system. Then, monthly data were composited by choosing the higher NDVI between two 15-daily datasets for each month. The 1 × 1-degree value was resampled into 2.5 × 2.5-degree grid system.

The GIMMS data are also adjusted for non-vegetative factors and represent interannual variation in vegetation well. The effects by stratospheric aerosol due to El Chichon and Mt. Pinatubo volcanic eruptions were adjusted. No correction for stratospheric ozone, Rayleigh scattering, and water vapor was considered. Cloud was screened according to 273°K of the brightness temperature of *Ch*5. Scan angle criteria is within +/– 40 degrees of nadir. Calibration for sensor degradation was executed based on an algorithm different from PAL [10, 2], and the desert correction. For the calibration of the orbital drift, Pinzon's [5] scheme was applied. Intercalibration with MODIS and SPOT/ VEGETATION was also conducted.

3) Evapotranspiration

Evapotranspiration from the land surface can be estimated from the atmospheric water budget [3]. ET from the bottom (i.e., land surface) of an air column, which vertically extends from the ground surface to the top of the atmosphere, can be expressed by the following atmospheric water budget equation:

$$ET = P + \frac{\partial W}{\partial t} + \nabla_H \cdot \vec{Q}$$

where t is the time, P is the precipitation at the bottom, W is the precipitable water in the air column, and $\nabla_H \cdot \vec{Q}$ is the horizontal flux divergence of water vapor integrated from the surface to the top of the atmosphere (so called aerial runoff).

This study assumed air columns above the 2.5 × 2.5-degree grid cells and computed each term for each grid cell. The CPC Merged Analysis of Precipitation (CMAP) dataset was used to determine monthly precipitation P [11]. The terms $\nabla_H \cdot \vec{Q}$ are computed from specific humidity and wind values. In the present study, these meteorological values were obtained from gridded 6-hourly atmospheric data (NCEP Reanalysis-2) provided by the National Centers for Environmental Prediction (NCEP) [1].

Monthly $\nabla_H \cdot \vec{Q}$ from 1982 to 2000 for each grid cell (192 × 94) of the reanalysis model was estimated by integrating the flux divergence from the ground to 0 hPa (all 28 layers of the model). The estimated values were interpolated onto the same 2.5 × 2.5-degree grid as the CMAP data. The monthly $\partial W / \partial t$ was calculated from the precipitable water difference between the beginning and end of each month.

3. Result and Discussion

1) Comparison of Geographical Distribution

The geographical distributions of PAL-NDVI and GIMMS-NDVI data values were compared and those in June are presented in Fig. 1. The NDVI distributions were essentially similar, showing high value over the boreal forest zone and low value over arid or low temperature regions such as deserts and tundra.

The absolute value of GIMMS-NDVI is generally

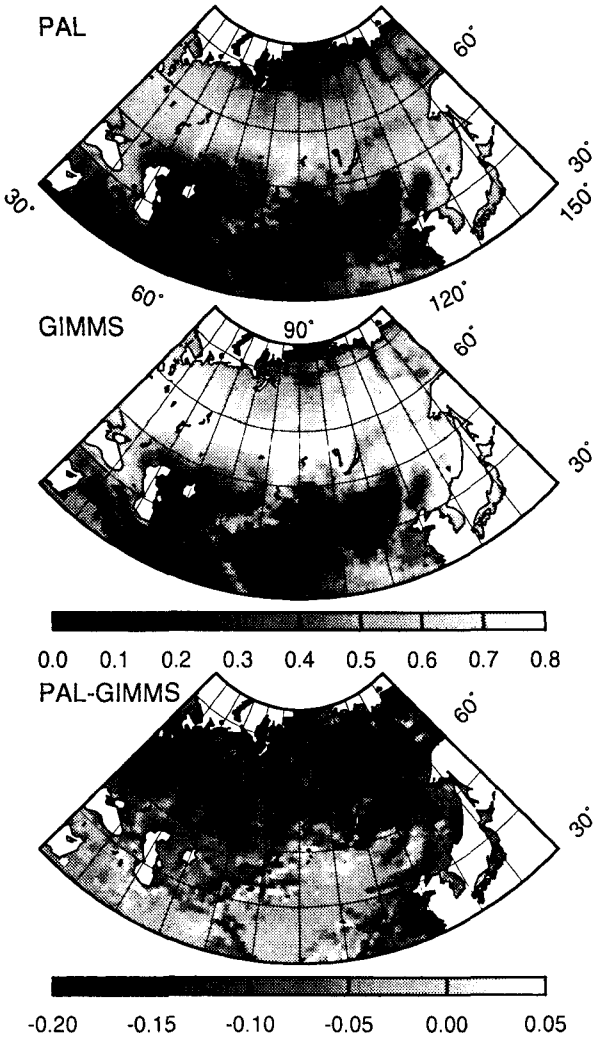

Fig. 1. Mean NDVI distribution in June averaged from 1982 to 2000. Top: PAL-NDVI, Mid: GIMMS-NDVI, Bottom: NDVI difference between PAL and GIMMS (PAL – GIMMS).

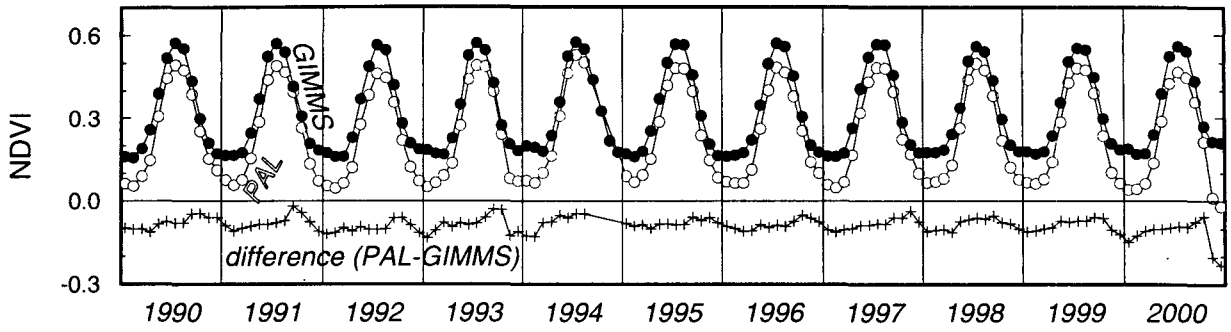

Fig.2. Mean temporal change of PAL-NDVI (open circle), GIMMS-NDVI (closed circle), and their difference (PAL – GIMMS) (cross) from 1990 to 2000 .

Table 1 Correlation coefficients of the PAL-NDVI and ET, GIMMS-NDVI and ET interannual changes from 1982 to 2000 for the three study regions; (a) Western Siberia (50°E – 90°E, 55°N – 65°N), (b) Eastern Siberia (80°E – 130°E, 65°N – 70°N), and (c) Kazakh (50°E – 60°E, 45°N – 55°N).

		Jan	Feb	Mar	Apr	May	Jun	Jul	Aug	Sep	Oct	Nov	Dec
Western Siberia	PAL	-0.02	-0.27	0.36	0.38	0.49	0.73	0.19	0.46	0.41	0.20	-0.51	0.00
	GIMMS	-0.04	0.09	0.19	0.35	0.53	0.66	0.61	0.52	0.34	0.09	-0.11	0.19
Eastern Siberia	PAL	-	0.03	0.22	-0.17	0.35	0.67	0.21	0.01	0.44	0.44	-	-
	GIMMS	-0.11	0.21	0.25	-0.48	0.33	0.71	0.40	0.14	0.15	0.02	0.15	0.18
Kazakh	PAL	-0.16	0.08	0.11	0.20	0.61	0.66	0.58	0.38	0.39	0.45	-0.12	0.28
	GIMMS	-0.15	0.29	0.17	0.02	0.55	0.64	0.50	0.32	0.20	0.33	0.09	0.08

higher than PAL-NDVI. Especially, GIMMS-NDVIs over northernmost area and local areas around Himalayas are much higher than PAL-NDVI as shown in Fig. 1. Although no picture is indicated, the PAL-NDVI inversely exhibits higher values than GIMMS-NDVI in the boreal forest zone singularly in October. It is considered that the data process of PAL or GIMMS in October is considerably different from other months.

2) *Comparison of Temporal Variation*

Fig. 2 demonstrates the time series of mean PAL-NDVI, GIMMS-NDVI and their difference from 1990 to 2000. Those variations are similar. Both NDVIs indicate striking seasonal change, that is, small value in winter and high value in summer, reflecting the vegetation phenology in the area. However GIMMS-NDVI indicates higher value than that of PAL-GIMMS throughout the year as known from the negative difference (PAL – GIMMS) value in Fig.2. Their difference tends to be small in autumn which is related to the larger PAL-NDVI than GIMMS-NDVI in October over boreal forest zone as aforementioned.

3) *Interannual Changes of NDVIs and ET*

Table 1 shows the correlation coefficients between 19-year interannual changes of mean PAL-NDVI and ET anomalies, and mean GIMMS-NDVI and ET anomalies in three representative regions for each month. Annually, the highest correlation was found in June in all three regions in both cases of PAL and GIMMS. Western Siberia has the highest coefficient (0.73) for PAL-NDVI in June, while the highest coefficient of GIMMS-NDVI is found in Eastern Siberia (0.71) in June. Since June is the most active season of vegetation, the highest correlation between NDVIs and ET is attributed to the greatest contribution of the vegetation transpiration to total ET in June. The fact that the highest coefficient occurs in June in both cases

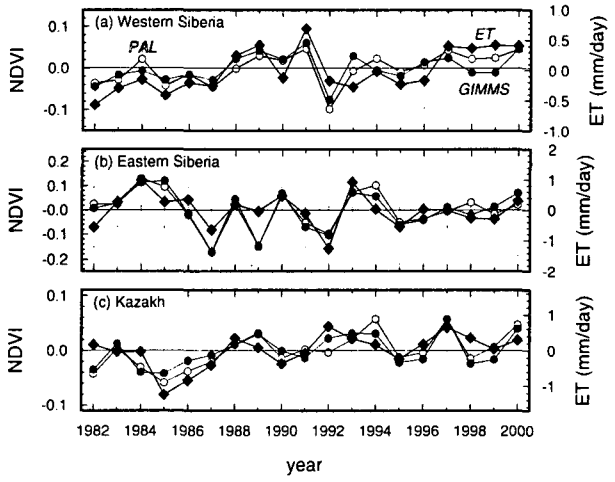

Fig.3. Interannual variation of the PAL-NDVI (open circle), GIMMS-NDVI (closed circle) and ET (diamond) anomalies averaged in the three selected regions. (*see* the caption of Table 1 for the longitude and latitude for these three regions).

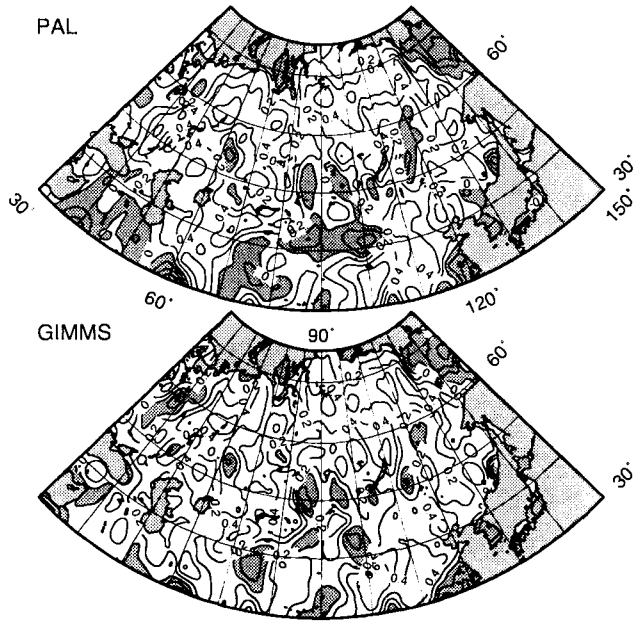

Fig.4. Distribution of the correlation coefficients between interannual changes of NDVI (upper: PAL-NDVI, lower: GIMMS-NDVI) and ET anomalies in June from 1982 to 2000. Areas with negative coefficient are shaded gray.

of PAL-NDVI and GIMMS-NDVI surely delineates the close interannual relationship between vegetation and ET.

19-year interannual changes (monthly anomalies) in the PAL-NDVI, GIMMS-NDVI, and ET in June, the month with the highest coefficient, over the three regions were indicated in Fig. 3. Very similar interannual changes among three parameters can be seen in each region. This result indicates that both PAL-NDVI and GIMMS-NDVI display similar interannual variation to ET for active growing season months.

Fig. 4 exhibits the geographical distribution of the correlation coefficient between 19-year interannual changes of PAL-NDVI and ET anomalies (upper) and GIMMS-NDVI and ET anolmaies (lower) in June. There are positive correlation coefficients over most regions of two maps, suggesting that interannual ET variation for most areas in Asia is affected by changes in vegetation. In arid and high altitude areas, small correlation coefficients (sometimes negative) are seen due to the very low NDVI in such areas in both cases of PAL and GIMMS.

4. Conclusion

PAL-NDVI and GIMMS-NDVI were both compared with interannual change in model-assimilated ET. Although the correlation coefficient between GIMMS-NDVI and ET is slightly less than for PAL-NDVI and ET, for both NDVI datasets the annual maximum correlation with ET occurs in June, which is near the central period of the growing season. A positive correlation between GIMMS-NDVI and ET was observed over most of the vegetated land area in June, and a similar result was obtained with PAL-NDVI. These results reinforce the authors' prior research that indicates the control of interannual change in ET is dominated by interannual change in vegetation activity.

References

[1] Kanamitsu, M., Ebisuzaki, W., Woollen, J., Yang, S.-K., Hnilo, J.J., Fiorino, M., and Potter, G.L., 2002, NCEP/DOE AMIP-II Reanalysis (R-2). *Bull. Amer. Meteor. Soc.*, 83, pp. 1631 – 1643.

[2] Los, S.O., 1998, Estimation of the ratio of sensor degradation between NOAA AVHRR channels 1 and 2 from monthly NDVI composites, *IEEE Trans. Geosci. Remote Sensing*, 36, pp. 206 – 213.

[3] Peixoto, J.P. and Oort, A.H., 1992, *Physics of Climate*, American Institute of Physics, NY.

[4] Pinzon, J., Brown M.E., and Tucker. C.J., 2004, Satellite time series correction of orbital drift artifacts using empirical mode decomposition. *In* Hilbert-Huang Transform: Introduction and Applications, N. Huang (eds.), Chapter 10, Part II. Applications (to appear).

[5] Pinzon, J., 2002, Using HHT to successfully uncouple seasonal and interannual components in remotely sensed data, *Proc. SCI 2002. Jul 14-18, Orlando*, Florida.

[6] Rao, C.R.N. and Chen, J., 1995, Inter-satellite calibration linkages for the visible and nearinfrared channels of the Advanced Very High Resolution Radiometer on the NOAA-7, -9, and -11 spacecraft, *Int. J. Remote Sensing*, 16, pp. 1931 – 1942.

[7] Rao, C.R.N. and Chen, J., 1996, Post-launch calibration of the visible and near-infrared channels of the advanced very high resolution radiometer on the NOAA-14 spacecraft, *Int. J. Remote Sensing*, 17, pp. 2743 – 2747.

[8] Suzuki, R., Masuda, K., 2004, Interannual covariability found in evapotranspiration and satellite-derived vegetation indices over northern Asia, *J. Meteor. Soc. Japan*, 82, pp 1233 – 1241.

[9] Tucker, C.J., Pinzon, J.E., Brown, M.E., Slayback, D., Pak, E.W., Mahoney, R., Vermote, E., and El Saleous, N., 2005, An extended AVHRR 8-km NDVI data set compatible with MODIS and SPOT vgetation NDVI data. *Int. J. Remote Sensing* (submitted)

[10] Vermote, E. and Kaufman, Y.J., 1995, Absolute calibration of AVHRR visible and nearinfrared channels using ocean and cloud views, *Int. J. Remote Sensing*, 16, pp. 2317 – 2340.

[11] Xie, P. and Arkin, P.A., 1997, Global precipitation: A 17-year monthly analysis based on gauge observations, satellite estimates, and numerical model outputs, *Bull. Amer. Meteor. Soc.*, 78, pp. 2539 – 2558.